Letter

Acoustic metafluids of shear modulus enabling surface waves

Sheng Zhang,[1] Yang Wang,[1] Manzhu Ke,[1,*] Fengming Liu,[2,†] Hailong He,[1] Liping Ye,[1] and Zhengyou Liu[1,3,‡]

[1]*Key Laboratory of Artificial Micro- and Nanostructures of Ministry of Education and School of Physics and Technology, Wuhan University, Wuhan 430072, China*

[2]*School of Mathematics and Physics, China University of Geosciences, Wuhan 430074, China*

[3]*Institute for Advanced Studies, Wuhan University, Wuhan 430072, China*

(Received 22 August 2022; revised 8 December 2022; accepted 12 December 2022; published 22 December 2022)

Metafluids, the version of metamaterials with fluid background, are generally characterized by two parameters: the effective mass density and bulk modulus. However, we recently theoretically demonstrated that a metafluid, with built-in quadrupolar resonances, can counterintuitively accommodate a third parameter, the effective shearlike modulus. In this letter, we go further to experimentally implement this metafluid, realized as a square lattice array of hollow steel cylinders in water. The effective parameters are extracted by matching the measured dispersion curves with the effective medium theory. By virtue of the emergent parameter, the metafluid can intrinsically support surface waves at the interface with water, which updates the knowledge that surface waves cannot exist at the interface of two fluids. Our work has potential in expanding the applications of metafluids.

DOI: 10.1103/PhysRevB.106.L220102

In the past two decades, great progress has been made in the development of acoustic metamaterials because of their manipulation functionalities on acoustic waves beyond the defined limits of those found in nature [1,2]. Acoustic metafluids are the version of acoustic metamaterials with fluid background, a concept which was proposed to describe artificial fluids with anisotropic mass density tensor [3–5]. Later, acoustic metafluids were generally seen as metamaterials with fluid background with abnormal parameters such as negative effective mass density [6–8], modulus [6,7,9], or anisotropic parameters [10]. Owning to the flexible regulation and design of the effective parameters, acoustic metafluids can offer many surprising possibilities for engineering sound waves in fluid such as negative refraction [6,7,11], acoustic subwavelength imaging [12,13], and acoustic cloaking [3,14–16].

Usually, acoustic metafluids (*metafluids* for short) acquire their abilities through the interaction between sound and various building units termed meta-atoms, which are remarkably smaller than the wavelength in the background medium in general. Therefore, metafluids can be described by effective parameters, and the wave propagation characteristics can be conveniently understood by using these effective parameters. It is known that, in conventional metafluids, the effective mass density and bulk modulus govern the propagation of acoustic waves, and the two parameters are associated with monopolar and dipolar scatterings, respectively [6,17]. In a recent work [18], we have theoretically shown that a metafluid consisting of periodic hollow solid cylinders immersed in fluid can provide, in addition to the effective mass density and bulk modulus, an effective parameter, i.e., effective shearlike modulus, which is determined by the strong quadrupolar resonances. However, this metafluid has not been realized in experiments, and its properties and applications have not been fully studied.

In this letter, we construct a metafluid using a square lattice array of hollow steel cylinders immersed in water. The band structures of the metafluid are measured experimentally, and the effective parameters are retrieved from these band structures. The experimental results validate our previous theory that the effective shearlike modulus can be introduced to describe the strong quadrupolar resonances of the metafluid. We extend the previous effective medium theory (EMT) [18] to characterize the metafluid as an anisotropic medium with effective stiffness tensor derived from the shearlike modulus. We further find that the interface between the metafluid and water can support surface waves, which updates the knowledge that surface waves cannot exist at the interface of two fluids. The dispersion curve of the surface wave can be obtained analytically using the effective stiffness tensor. It is also found that the dispersion curve changes with the angle between the principal axis of the stiffness tensor and the interface. This surface wave is completely different from the previous surface states in acoustic metamaterials that require a negative effective mass density [19,20] and from spoof acoustic surface waves propagating along a corrugated rigid surface [21–26]. Finally, we perform experiments to measure the dispersion curve and pressure field distribution of the surface wave. The experimental results are in good agreement with the analytical and simulated results.

The experimental metafluid with effective shearlike modulus is shown in Fig. 1(a). The unit cell of the metafluid consists of a hollow steel ($\rho = 7670\,\mathrm{kg/m^3}$, $c_l = 6010\,\mathrm{m/s}$, and $c_t = 3230\,\mathrm{m/s}$) cylinder ($R = 0.53$ mm and $r = 0.415$ mm) immersed in water ($\rho_0 = 1000\,\mathrm{kg/m^3}$ and $\kappa_0 = 2.22$ GPa). Since the length of the cylinder along the z axis is much larger than the acoustic wavelength of water in the frequency range of interest, the experimental metafluid can be considered as a

*mzke@whu.edu.cn
†liufm@cug.edu.cn
‡zyliu@whu.edu.cn

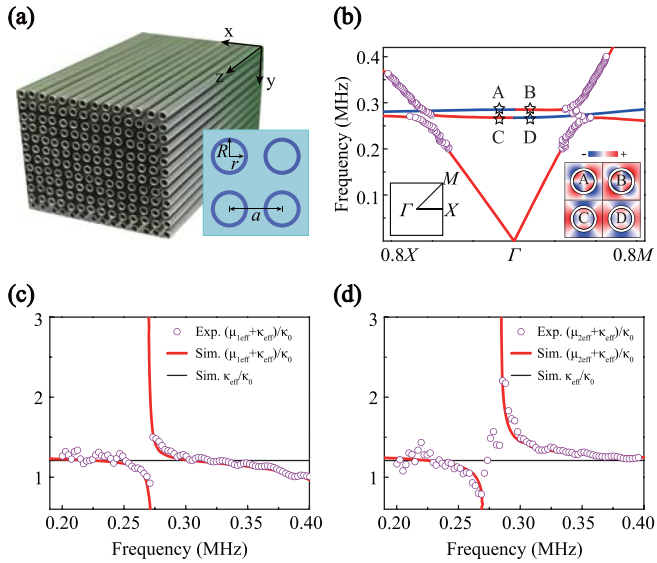

FIG. 1. Experimental realization of the metafluid with effective shearlike modulus. (a) The metafluid consisting of square lattice hollow steel cylinders with $R = 0.53$ mm, $r = 0.415$ mm, and $a = 1.5$ mm. (b) Experimentally measured and numerically simulated band structures of the metafluid. The solid lines denote the numerical results (red for active branches and blue for uncoupled branches). The purple circles denote the experimental results. The inset shows pressure field distributions of the eigenmodes corresponding to A–D labeled on the band structures. (c) and (d) Effective parameters retrieved from the experimental and numerical band structures along the ΓX and ΓM directions, respectively. All effective parameters have been normalized to the acoustic parameters of water.

two-dimensional (2D) system. We choose the parameters of this metafluid because they possess a clean quadrupolar mode without the interference of the monopolar and dipolar modes. Figure 1(b) shows the experimentally measured (purple circles) and numerically simulated (red and blue solid lines) band structures of the metafluid. There are two flat bands associated with the quadrupolar resonances indicated by the pressure field distributions of the eigenmodes in Fig. 1(b). These bands exhibit anisotropic coupling behavior with the linear band starting from zero frequency. The lower frequency flat band couples with the linear band along the ΓX direction and does not along the ΓM direction, whereas the opposite occurs for the higher frequency flat band. The group theory analysis of the symmetry of eigenmodes has been used to explain the anisotropic coupling behavior of the quadrupolar bands with the linear band [18,27,28]. When the pressure field of the quadrupolar mode is symmetric along the $\Gamma X/\Gamma M$ direction (shown in the field distribution C/B), the corresponding shearlike modulus $\mu_{1\mathrm{eff}}/\mu_{2\mathrm{eff}}$ is generated [shown in Figs. 1(c) and 1(d)]. Note that only the active branches can be measured in the experiment since the incident plane wave cannot excite the uncoupled branches. Our previous EMT has succeeded in describing the low-frequency quadrupolar resonances, which can be used to reproduce the main features of the band structures by introducing the effective shearlike modulus [18]. As described in our previous work, the dispersion of the active branch in the ΓX direction is expressed as

$$(k_{1L})^2 = \omega^2 \frac{\rho_{\mathrm{eff}}}{\mu_{1\mathrm{eff}} + \kappa_{\mathrm{eff}}}, \tag{1}$$

and the dispersion of the active branch in the ΓM direction is expressed as

$$(k_{2L})^2 = \omega^2 \frac{\rho_{\mathrm{eff}}}{\mu_{2\mathrm{eff}} + \kappa_{\mathrm{eff}}}. \tag{2}$$

Figures 1(c) and 1(d) show the retrieved effective shearlike modulus and bulk modulus from the experimental and numerical band structures along the ΓX and ΓM directions, respectively. Two shearlike moduli $\mu_{1\mathrm{eff}}$ and $\mu_{2\mathrm{eff}}$ are related to the two nondegenerate quadrupolar resonance modes in the square lattice metafluid. They only play a significant role near the resonance frequencies. The perfect consistency between the experimental and the numerical results affirms the realization of the metafluid with the shearlike modulus.

We note that, in our previous EMT, the shearlike moduli $\mu_{1\mathrm{eff}}$ and $\mu_{2\mathrm{eff}}$ can only be used to describe the acoustic wave-propagation characteristics in the high-symmetry directions for the metafluid with a square lattice. Here, we would like to extend the previous EMT to characterize the metafluid for arbitrary propagation directions. Because the metafluid exhibits anisotropic properties, it is natural to introduce the stiffness constants C_{11}, C_{12}, and C_{66} for this metafluid. By comparing the wave velocity equations calculated by the constitutive relation and Newton's second law with Eqs. (1) and (2), the unknown stiffness constants C_{11}, C_{12}, and C_{66} can be derived as a function of the effective parameters $\mu_{1\mathrm{eff}}$, $\mu_{2\mathrm{eff}}$, and κ_{eff}. More details are shown in the Supplemental Material [29] (see also Ref. [30] therein). Thus, the metafluid can be mapped to an effective anisotropic medium (EAM) with the effective stiffness tensor:

$$[C] = \begin{pmatrix} C_{11} & C_{12} & 0 \\ C_{12} & C_{11} & 0 \\ 0 & 0 & C_{66} \end{pmatrix} = \begin{pmatrix} \kappa_{\mathrm{eff}} + \mu_{1\mathrm{eff}} & \kappa_{\mathrm{eff}} - \mu_{1\mathrm{eff}} & 0 \\ \kappa_{\mathrm{eff}} - \mu_{1\mathrm{eff}} & \kappa_{\mathrm{eff}} + \mu_{1\mathrm{eff}} & 0 \\ 0 & 0 & \mu_{2\mathrm{eff}} \end{pmatrix}, \tag{3}$$

to note that the effective medium description is generally suitable in the subwavelength limit. By virtue of the effective stiffness tensor, the dispersions and the associated modes of the metafluid can be obtained from Christoffel's equation [31].

According to the above analysis, Fig. 2 shows the mapping of the metafluid to an EAM. As an example, Fig. 2(b) shows the slowness surfaces of the equivalent anisotropic medium at a frequency of 0.277 MHz.

It is well known that there are many different types of surface acoustic waves [32] depending on the nature of the two media forming the interface, such as solid-solid and solid-fluid interfaces. Surface waves in acoustic metamaterials are closely analogous to a surface plasmon polariton in the optical case. They exist either at the interface between two semi-infinite homogeneous fluids with different signs of effective mass density [19,20] or on the rigid surface artificially modulated with arrays of subwavelength grooves or holes [21–26]. However, since our metafluid possesses unique effective stiffness tensor and positive effective mass

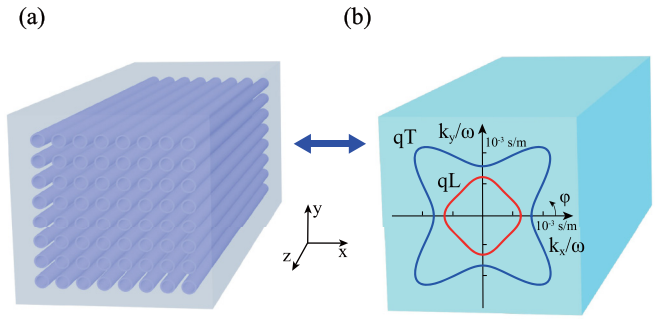

FIG. 2. Mapping the metafluid to an effective anisotropic medium (EAM). (a) Schematic of the metafluid consisting of hollow steel cylinders immersed in water. (b) The equivalent anisotropic medium and its slowness surfaces at a frequency of 0.277 MHz. The red and blue lines represent quasilongitudinal and quasitransverse waves, respectively.

density (Supplemental Material [29]), we will explore whether the metafluid can support Rayleigh-like surface wave.

Figure 3(a) shows the schematic of the analytical model for thoroughly investigating the dispersion of the surface wave by using the effective stiffness tensor. Semi-infinite medium I is the EAM and medium II is water. The 2D constitutive relation of the EAM in a global coordinate xoy can be expressed as

$$\begin{pmatrix} T_{xx} \\ T_{yy} \\ T_{xy} \end{pmatrix} = \begin{pmatrix} C'_{11} & C'_{12} & C'_{16} \\ C'_{12} & C'_{11} & C'_{26} \\ C'_{16} & C'_{26} & C'_{66} \end{pmatrix} \begin{pmatrix} S_{xx} \\ S_{yy} \\ 2S_{xy} \end{pmatrix}. \tag{4}$$

Here, $[C']$ is the general stiffness matrix which can be obtained from the effective stiffness tensor [Eq. (3)] in the principle coordinate system by the coordinate transformation:

$$\begin{pmatrix} C'_{11} & C'_{12} & C'_{16} \\ C'_{12} & C'_{11} & C'_{26} \\ C'_{16} & C'_{26} & C'_{66} \end{pmatrix} = [N] \begin{pmatrix} C_{11} & C_{12} & 0 \\ C_{12} & C_{11} & 0 \\ 0 & 0 & C_{66} \end{pmatrix} [N]^T, \tag{5}$$

where

$$[N] = \begin{pmatrix} \cos^2\theta & \sin^2\theta & \sin 2\theta \\ \sin^2\theta & \cos^2\theta & -\sin 2\theta \\ -\sin\theta\cos\theta & \sin\theta\cos\theta & \cos^2\theta - \sin^2\theta \end{pmatrix}$$

is the coordinate transformation matrix, and θ denotes a rotation angle of the principal axis with respect to the y axis in the global coordinate. The displacement field in the EAM is

$$\mathbf{u} = \begin{pmatrix} u_x \\ u_y \end{pmatrix} = \begin{pmatrix} u_x^0 \\ u_y^0 \end{pmatrix} \exp(ik_x x) \exp(ik_y y) \exp(-i\omega t), \tag{6}$$

where u_x^0 and u_y^0 are the displacement polarizations, k_x and k_y are the wave numbers along the x and y axes, respectively, and ω is the circular frequency. By substituting the displacement field into the dynamic elasticity equation $-\omega^2\rho_{\text{eff}}\mathbf{u} = \nabla \cdot \mathbf{T}$, the eigenvalue equation can be obtained [31]:

$$\begin{bmatrix} C'_{11}k_x^2 + C'_{66}k_y^2 + 2C'_{16}k_xk_y - \rho_{\text{eff}}\omega^2 & C'_{16}k_x^2 + C'_{26}k_y^2 + (C'_{12} + C'_{66})k_xk_y \\ C'_{16}k_x^2 + C'_{26}k_y^2 + (C'_{12} + C'_{66})k_xk_y & C'_{66}k_x^2 + C'_{11}k_y^2 + 2C'_{26}k_xk_y - \rho_{\text{eff}}\omega^2 \end{bmatrix} \begin{pmatrix} u_x \\ u_y \end{pmatrix} = 0. \tag{7}$$

We can get two dispersion relations from the above equation, one corresponding to the quasilongitudinal (qL) mode and the other to the quasitransverse (qT) mode:

$$2\rho_{\text{eff}}\omega^2 = (C'_{11} + C'_{66})\left(k_{xqL}^2 + k_{yqL}^2\right) + \sqrt{\Delta_{qL}}, \tag{8}$$

$$2\rho_{\text{eff}}\omega^2 = (C'_{11} + C'_{66})\left(k_{xqT}^2 + k_{yqT}^2\right) - \sqrt{\Delta_{qT}}, \tag{9}$$

$$\Delta_{qL} = \left[(C'_{11} - C'_{66})\left(k_{xqL}^2 - k_{yqL}^2\right) + 4C'_{16}k_{xqL}k_{yqL}\right]^2 + 4\left[C'_{16}\left(k_{xqL}^2 - k_{yqL}^2\right) + (C'_{12} + C'_{66})k_{xqL}k_{yqL}\right]^2, \tag{10}$$

$$\Delta_{qT} = \left[(C'_{11} - C'_{66})\left(k_{xqT}^2 - k_{yqT}^2\right) + 4C'_{16}k_{xqT}k_{yqT}\right]^2 + 4\left[C'_{16}\left(k_{xqT}^2 - k_{yqT}^2\right) + (C'_{12} + C'_{66})k_{xqT}k_{yqT}\right]^2. \tag{11}$$

Displacement fields for the qL and qT modes are

$$\boldsymbol{u}_{qL} = \begin{pmatrix} 1 \\ \tan\beta_{qL} \end{pmatrix} \exp(ik_{xqL}x) \exp(ik_{yqL}y) \exp(-i\omega t), \tag{12}$$

$$\boldsymbol{u}_{qT} = \begin{pmatrix} 1 \\ \tan\beta_{qT} \end{pmatrix} \exp(ik_{xqT}x) \exp(ik_{yqT}y) \exp(-i\omega t), \tag{13}$$

respectively. Thus, the total displacement field in the EAM is in the form of $\boldsymbol{u} = M_{qL}\boldsymbol{u}_{qL} + M_{qT}\boldsymbol{u}_{qT}$,

$$\begin{aligned} u_x &= M_{qL} \exp(ik_{xqL}x) \exp(ik_{yqL}y) \exp(-i\omega t) \\ &\quad + M_{qT} \exp(ik_{xqT}x) \exp(ik_{yqT}y) \exp(-i\omega t), \\ u_y &= M_{qL} \tan\beta_{qL} \exp(ik_{xqL}x) \exp(ik_{yqL}y) \exp(-i\omega t) \\ &\quad + M_{qT} \tan\beta_{qT} \exp(ik_{xqT}x) \exp(ik_{yqT}y) \exp(-i\omega t), \end{aligned} \tag{14}$$

where M_{qL} and M_{qT} are the amplitudes of the qL and qT modes. We write the displacement field in water as

$$\boldsymbol{u}_0 = \begin{pmatrix} 1 \\ \frac{k_{y0}}{k_{x0}} \end{pmatrix} \exp(ik_{x0}x) \exp(ik_{y0}y) \exp(-i\omega t).$$

Here $k_{x0}^2 + k_{y0}^2 = k_0^2 = \frac{\omega^2}{c_0^2}$, and c_0 is the wave speed of water. We study the surface wave propagating along the x axis in the global coordinate xoy, so the wave numbers k_x of all the displacement fields should be coincident [33]. Thus, the

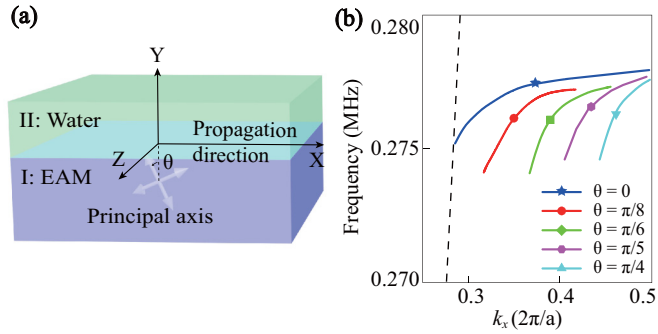

FIG. 3. The surface wave at the interface between the semi-infinite metafluid and water. (a) Schematic of the analytical model for analyzing the surface wave. The metafluid is mapped to an effective anisotropic medium (EAM) with the principal axis orientated at an angle θ with respect to the y axis in the global coordinate. (b) Analytically obtained dispersion curves of the surface wave for different rotation angles θ. The black dashed line denotes the water line.

displacement fields in the EAM and water can be obtained:

$$
\begin{aligned}
u_x^{\mathrm{I}} &= M_{qL}\exp(ik_x x)\exp(ik_{yqL}y)\exp(-i\omega t) \\
&\quad + M_{qT}\exp(ik_x x)\exp(ik_{yqT}y)\exp(-i\omega t), \\
u_y^{\mathrm{I}} &= M_{qL}\tan\beta_{qL}\exp(ik_x x)\exp(ik_{yqL}y)\exp(-i\omega t) \\
&\quad + M_{qT}\tan\beta_{qT}\exp(ik_x x)\exp(ik_{yqT}y)\exp(-i\omega t), \\
u_x^{\mathrm{II}} &= M_0\exp(ik_x x)\exp(ik_{y0}y)\exp(-i\omega t), \\
u_y^{\mathrm{II}} &= M_0\frac{k_{y0}}{k_x}\exp(ik_x x)\exp(ik_{y0}y)\exp(-i\omega t). \qquad (15)
\end{aligned}
$$

By considering the continuous conditions, we can calculate the dispersion curve of the surface wave by solving the derived secular equation. Figure 3(b) shows the dispersion curves of the surface wave for different rotation angles θ. The results not only confirm the existence of the surface wave at the interface between the metafluid and water but also exhibit intriguing dispersion features. The dispersion curve changes significantly with the rotation of the principal axis, which is not achievable in conventional acoustic metamaterials. Thus, we have found a way to manipulate acoustic surface waves.

To verify the above theoretical analysis, we experimentally measure the dispersion and pressure field distribution of the surface wave. Figure 4(a) shows the schematic of the experimental setup. The metafluid sample consists of 38 × 16 unit cells and is placed in a water tank. An incident plane wave is injected on the interface between the water and the metafluid sample at an angle of 75°, and a probe can be applied to record the pressure field distribution by scanning the surface above the metafluid. Through the Fourier transformation of the pressure fields, the dispersion of the surface wave can be obtained. More experimental details are shown in the Supplemental Material [29]. Figure 4(b) shows the dispersions of the surface wave along the k_x direction. The color maps represent the experimental results, while the cyan dotted line is the result of full-wave simulation by the supercell method. The dispersion curve of the surface wave lies in the projected bands gap and below the water line (black dashed line). In addition, the analytically calculated dispersion curve of the surface wave (the blue solid line located in the red dashed box

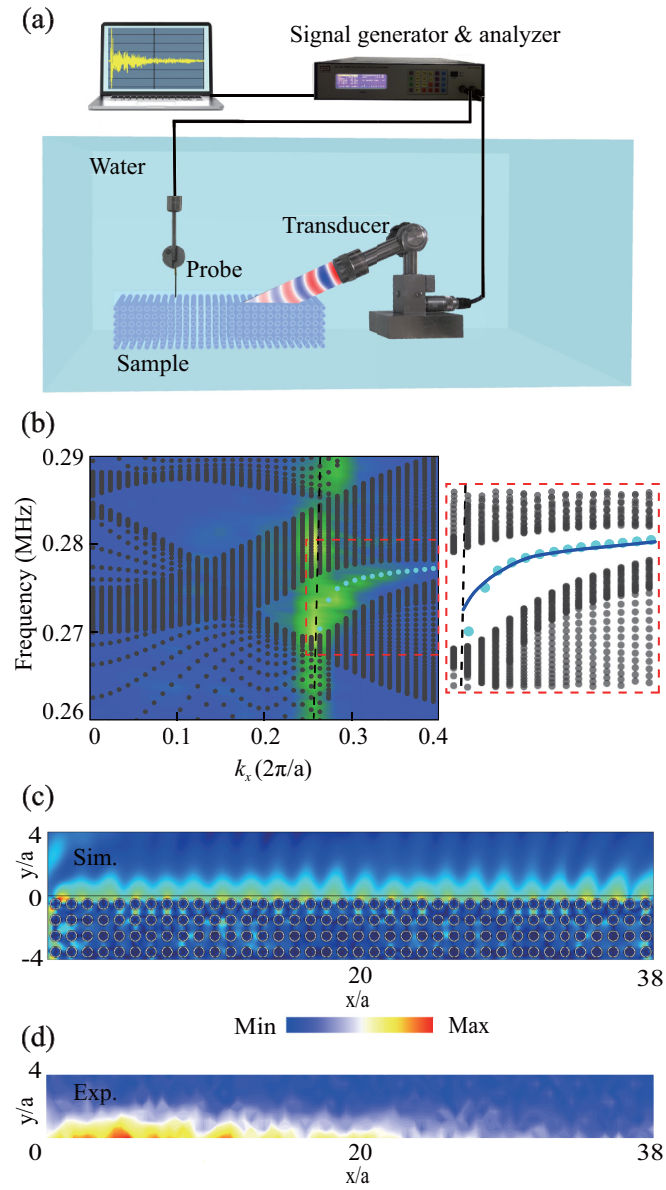

FIG. 4. Experimental demonstration of the surface wave at the interface between the metafluid and water. (a) Schematic of the experimental setup. (b) The dispersions of the surface wave. The color maps represent the measured data, the cyan and black dotted lines denote the simulated dispersions of the surface wave and projected bulk states, and the right panel (enlarged view of the red dashed box in the left panel) shows the analytical calculation result with a blue solid line. The black dashed line denotes the water line. (c) The simulated pressure field distributions of the surface wave outside and inside the metafluid at the frequency of 0.274 MHz. (d) The experimental pressure field distribution of the surface wave outside the metafluid at the same frequency.

in the right panel) is plotted in Fig. 4(b). All results obtained in three different ways agree well over most of the range of k_x, which strongly indicates that the metafluid can intrinsically support surface acoustic waves at the interface with water. To show more intuitive properties of the surface wave, we further give the simulated and measured field distributions [Figs. 4(c) and 4(d), f = 0.274 MHz] in real space near the interface. We

can clearly see that the pressure fields decay in both water and the metafluid perpendicular to the interface in Fig. 4(c). The experimental measured field distribution in Fig. 4(d) also shows the same attenuation characteristic in water. It should be noted that it is too difficult for the experimental operation to observe the field distribution inside the metafluid. The localized pressure fields at the interface evidently exhibit the characteristics of surface waves. Due to the unavoidable loss in the experiment, the measured surface wave [Fig. 4(d)] decays fast after propagating ∼22 units as compared with the simulated result [Fig. 4(c)]. The experimental results still agree well with the numerical results.

In conclusion, we have experimentally implemented an acoustic metafluid with effective shearlike modulus which consists of a square lattice array of hollow steel cylinders in water. We have also extended the previous EMT to characterize our metafluid as an EAM with effective stiffness tensor derived from the shearlike modulus. By virtue of the emergent parameter, we further indicate that the metafluid can intrinsically support Rayleigh-like surface wave at the interface with water, which updates the knowledge that surface waves cannot exist at the interface of two fluids. The theoretical prediction of the surface wave between water and the metafluid has been perfectly demonstrated by experimental measurements of the dispersion curve and pressure field distributions near the interface. Our work not only updates the traditional knowledge of fluid but also has potential in expanding the applications of metafluids.

This letter is supported by the National Key R&D Program of China (Grant No. 2018YFA0305800), the National Natural Science Foundation of China (Grants No. 11890701, No. 11974262, No. 12174353, No. 12004286, and No. 12104347), and the China Postdoctoral Science Foundation (Grants No. BX20200259, No. 2020TQ0233, No. 2020M682461, and No. 2020M682462).

[1] Z. Liu, X. Zhang, Y. Mao, Y. Zhu, Z. Yang, C. T. Chan, and P. Sheng, Locally resonant sonic materials, Science **289**, 1734 (2000).
[2] G. Ma and P. Sheng, Acoustic metamaterials: from local resonances to broad horizons, Sci. Adv. **2**, el501595 (2016).
[3] J. Pendry and J. Li, An acoustic metafluid: realizing a broadband acoustic cloak, New J. Phys. **10**, 115032 (2008).
[4] A. N. Norris, Acoustic metafluids, J. Acoust. Soc. Am. **125**, 839 (2009).
[5] D. Torrent and J. Sánchez-Dehesa, Sound scattering by anisotropic metafluids based on two-dimensional sonic crystals, Phys. Rev. B **79**, 174104 (2009).
[6] J. Li and C. T. Chan, Double-negative acoustic metamaterial, Phys. Rev. E **70**, 055602(R) (2004).
[7] Z. Liang and J. Li, Extreme Acoustic Metamaterial by Coiling Up Space, Phys. Rev. Lett. **108**, 114301 (2012).
[8] J. Mei, Z. Liu, W. Wen, and P. Sheng, Effective dynamic mass density of composites, Phys. Rev. B **76**, 134205 (2007).
[9] N. Fang, D. Xi, J. Xu, M. Ambati, W. Srituravanich, C. Sun, and X. Zhang, Ultrasonic metamaterials with negative modulus, Nat. Mater. **5**, 452 (2006).
[10] J. Christensen and F. J. G. de Abajo, Anisotropic Metamaterials for Full Control of Acoustic Waves, Phys. Rev. Lett. **108**, 124301 (2012).
[11] S. Wang, G. Zhang, X. Wang, Q. Tong, J. Li, and G. Ma, Spin-orbit interactions of transverse sound, Nat. Commun. **12**, 6125 (2021).
[12] A. Sukhovich, B. Merheb, K. Muralidharan, J. O. Vasseur, Y. Pennec, P. A. Deymier, and J. H. Page, Experimental and Theoretical Evidence for Subwavelength Imaging in Phononic Crystals, Phys. Rev. Lett. **102**, 154301 (2009).
[13] M. Molerón and C. Daraio, Acoustic metamaterial for subwavelength edge detection, Nat. Commun. **6**, 8037 (2015).
[14] S. A. Cummer and D. Schurig, One path to acoustic cloaking, New J. Phys. **9**, 45 (2007).
[15] H. Chen and C. T. Chan, Acoustic cloaking and transformation acoustics, J. Phys. D **43**, 113001 (2010).
[16] S. Zhang, C. Xia, and N. Fang, Broadband Acoustic Cloak for Ultrasound Waves, Phys. Rev. Lett. **106**, 024301 (2011).
[17] S. H. Lee and O. B. Wright, Origin of negative density and modulus in acoustic metamaterials, Phys. Rev. B **93**, 024302 (2016).
[18] F. Liu, Z. Wang, M. Ke, and Z. Liu, Metafluids Beyond the Bulk Modulus, Phys. Rev. Lett. **125**, 185502 (2020).
[19] M. Ambati, N. Fang, C. Sun, and X. Zhang, Surface resonant states and superlensing in acoustic metamaterials, Phys. Rev. B **75**, 195447 (2007).
[20] C. Shen, J. Xu, N. Fang, and Y. Jing, Anisotropic Complementary Acoustic Metamaterial for Canceling Out Aberrating Layers, Phys. Rev. X **4**, 041033 (2014).
[21] L. Kelders, J. F. Allard, and W. Lauriks, Ultrasonic surface waves above rectangular-groove gratings, J. Acoust. Soc. Am. **103**, 2730 (1998).
[22] J. Christensen, A. I. Fernandez-Dominguez, F. de Leon-Perez, L. Martin-Moreno, and F. J. Garcia-Vidal, Collimation of sound assisted by acoustic surface waves, Nat. Phys. **3**, 851 (2007).
[23] D. Zhao, Z. Liu, C. Qiu, Z. He, F. Cai, and M. Ke, Surface acoustic waves in two-dimensional phononic crystals: Dispersion relation and the eigenfield distribution of surface modes, Phys. Rev. B **76**, 144301 (2007).
[24] Y. Zhou, M. Lu, L. Feng, X. Ni, Y. Chen, Y. Zhu, S. Zhu, and N. Ming, Acoustic Surface Evanescent Wave and Its Dominant Contribution to Extraordinary Acoustic Transmission and Collimation of Sound, Phys. Rev. Lett. **104**, 164301 (2010).
[25] L. Wu, G. Song, W. Cao, Q. Cheng, T. Cui, and Y. Jing, Generation of multiband spoof surface acoustic waves via high-order modes, Phys. Rev. B **97**, 214305 (2018).
[26] N. Cselyuszka, A. Alù, and N. Janković, Spoof-Fluid-Spoof Acoustic Waveguide and Its Applications for Sound Manipulation, Phys. Rev. Appl. **12**, 054014 (2019).

[27] K. Sakoda, Symmetry, degeneracy, and uncoupled modes in two-dimensional photonic lattices, Phys. Rev. B **52**, 7982 (1995).

[28] Y. Wu and Z. Zhang, Dispersion relations and their symmetry properties of electromagnetic and elastic metamaterials in two dimensions, Phys. Rev. B **79**, 195111 (2009).

[29] See Supplemental Material at http://link.aps.org/supplemental/10.1103/PhysRevB.106.L220102 for the extended EMT, the effective mass density of the metafluid, and details of the experiments.

[30] Y. Lai, Y. Wu, P. Sheng, and Z. Zhang, Hybrid elastic solids, Nat. Mater. **10**, 620 (2011).

[31] D. Royer and E. Dieulesaint, *Elastic Waves in Solids I* (Springer, New York, 1999).

[32] P. Hess, Surface acoustic waves in materials science, Phys. Today **55**, 42 (2002).

[33] N. Favretto-Cristini, D. Komatitsch, J. M. Carcione, and F. Cavallini, Elastic surface waves in crystals. Part 1: review of the physics, Ultrasonics **51**, 653 (2011).